Saudi Pharmaceutical Journal 28 (2020) 1420–1430

Contents lists available at ScienceDirect

Saudi Pharmaceutical Journal

journal homepage: www.sciencedirect.com

Original article

Dual-action of thermoresponsive gels containing DsiRNA-loaded gold nanoparticles for diabetic wound therapy: Characterization, *in vitro* safety and healing efficacy

Ahmad Yasser Hamdi Nor Azlan [a,b], Haliza Katas [a,*], Nur Hamizah Habideen [a], Mohd Fauzi Mh Busra [c]

[a] Centre for Drug Delivery Research, Faculty of Pharmacy, Universiti Kebangsaan Malaysia, Jalan Raja Muda Abdul Aziz, Kuala Lumpur, Malaysia
[b] Faculty of Pharmacy and Health Sciences, Universiti Kuala Lumpur (Royal College of Medicine Perak), 3, Jalan Greentown, 30450 Ipoh, Perak, Malaysia
[c] Tissue Engineering Centre, UKM Medical Centre, 56000 Cheras, Kuala Lumpur, Malaysia

ARTICLE INFO

Article history:
Received 22 April 2020
Accepted 11 September 2020
Available online 18 September 2020

Keywords:
Green synthesis
Metal nanoparticles
Diabetes mellitus
Antimicrobial agent
RNA interfering
Gene silencing

ABSTRACT

Diabetic wounds are difficult to treat due to multiple causes, including reduced blood flow and bacterial infections. Reduced blood flow is associated with overexpression of prostaglandin transporter (PGT) gene, induced by hyperglycaemia which causing poor vascularization and healing of the wound. Recently, gold nanoparticles (AuNPs) have been biosynthesized using cold and hot sclerotium of *Lignosus rhinocerotis* extracts (CLRE and HLRE, respectively) and capped with chitosan (CS) to produce biocompatible antibacterial nanocomposites. The AuNPs have shown to produce biostatic effects against selected gram positive and negative bacteria. Therefore, in this study, a dual therapy for diabetic wound consisting Dicer substract small interfering RNA (DsiRNA) and AuNPs was developed to improve vascularization by inhibiting PGT gene expression and preventing bacterial infection, respectively. The nanocomposites were incorporated into thermoresponsive gel, made of pluronic and polyethylene glycol. The particle size of AuNPs synthesized using CLRE (AuNPs-CLRE) and HLRE (AuNPs-HLRE) was 202 ± 49 and 190 ± 31 nm, respectively with positive surface charge (+30 to + 45 mV). The thermoresponsive gels containing DsiRNA-AuNPs gelled at 32 ± 1 °C and released the active agents in sufficient amount with good texture and rheological profiles for topical application. DsiRNA-AuNPs and those incorporated into thermoresponsive pluronic gels demonstrated high cell viability, proliferation and cell migration rate via *in vitro* cultured cells of human dermal fibroblasts, indicating their non-cytotoxicity and wound healing properties. Taken together, the thermoresponsive gels are expected to be useful as a potential dressing that promotes healing of diabetic wounds.

1. Introduction

Slow healing of diabetic wounds is caused by multiple factors, including peripheral neuropathy, reduced blood flow and bacterial infections, all of which occur with higher frequency and intensity in diabetic population. Elevated blood sugar level stiffens and narrows blood vessels, restricting the delivery of oxygen and nutrients that are important for natural healing ability (Nimasajai, 2018). The elevated blood glucose level has been also associated with reduced blood flow at the wound site of diabetic patients by up-regulating prostaglandin transporter (PGT) gene. Overexpression of PGT gene reduces the production of prostaglandin E2 (PGE2), a prostaglandin that enhances angiogenesis (Syeda et al., 2012). Moreover, PGT overexpression mediates defects in endothelial and peripheral vascular function (Rissanen et al., 2001; Dalla & Faglia, 2006; Kavitha, 2014) that slowing the healing of diabetic wound. The wounds may also be complicated by bacterial infections which represents an important challenge in the development of efficient therapy.

A dual-action therapy consisting agents with healing properties and antibacterial activity is a good strategy to treat diabetic wounds. In present study, a therapy to promote vascularization

* Corresponding author at: Centre for Drug Delivery Research, Faculty of Pharmacy, Universiti Kebangsaan Malaysia, Kuala Lumpur Campus, Jalan Raja Muda Abdul Aziz, 50300 Kuala Lumpur, Malaysia.
E-mail addresses: p93200@siswa.ukm.edu.my (A.Y.H. Nor Azlan), haliza.katas@ukm.edu.my (H. Katas), myza_5796@yahoo.com (N.H. Habideen), fauzibusra@ukm.edu.my (M.F. Mh Busra).

Peer review under responsibility of King Saud University.

Production and hosting by Elsevier

https://doi.org/10.1016/j.jsps.2020.09.007
1319-0164/

and prevent infection was developed by integrating Dicer-substrate small interfering RNA (DsiRNA) and gold nanoparticles (AuNPs) as a nanocomposite. In diabetes mellitus, PGT up-regulation could be corrected by silencing the gene using DsiRNA, a RNAi-based therapeutic agent. Previously, AuNPs as an antibacterial component were produced via green synthesis using aqueous extract of sclerotium of *Lignosus rhinocerotis,* also known as tiger milk mushroom (Katas et al., 2019). Based on the traditional use of *Lignosus rhinocerotis* in inducing wound healing as well as a recent finding on polysaccharides content in its extracts (Katas et al. 2019), the investigation of its potential in promoting wound healing is paramount. Biologically active compounds such as some plant polysaccharides have been reported to affect different phases of wound healing (Zhang et al. 2019), showing the potential of *Lignosus rhinocerotis* extracts as one of the sources for compounds with healing properties. Chitosan (CS) was used as a capping agent (stabilizing) of the resultant AuNPs due to their good combination of properties such as biodegradable, biocompatible, and non-toxic. The nanocomposites exhibited antibacterial activity against selected gram positive and negative bacteria. The addition of CS also enhanced the antibacterial activity of AuNPs due to the synergistic effect of both as CS poses antibacterial property (Sarwar et al., 2015; Biranje et al., 2019).

In present study, DsiRNA-loaded AuNPs, synthesized using CLRE and HLRE were incorporated into thermoresponsive gels prepared from pluronic (PF-127), a polymer that converts into gel at body temperature (Katas et al., 2017). PF-127 was used to prepare the thermoresponsive gel owing to its ability in improving drug permeation through the skin (Lee et al., 2014). Besides, it has a low toxicity, making it suitable to be developed as a wound dressing. The nanocomposites and gels were characterized for physical characteristics, rheological and drug release behaviours. Cytotoxicity effect and proliferation as well as migration rate of cells after exposing to the AuNPs and gels were also determined via *in vitro* cultured human dermal fibroblasts (HDFs). The gels demonstrated as an effective healing accelerator, offering a new promising strategy for diabetic wound therapy in future.

2. Materials and methods

2.1. Materials

Gold (III) chloride hydrate (99.999% trace metals basis) was purchased from Sigma-Aldrich (Malaysia). Sodium citrate tribasic dihydrate was purchased from Sigma-Aldrich (Ireland). *L. rhinocerotis* sclerotial powder was provided as a gift from Lignas Bio Synergy Plt., Selangor, Malaysia. DsiRNA targeting PGT gene [5′-rGrArArGrGrArArGrUrGrGrCrUrGrArGrUrUrArUrUrArATA-3′ (sense strand) and rUrArUrUrArArUrUrArCrUrCrArGrCrCrArCrUrUrCrCrUrUrCrUrU (antisense strand)] of 27 bp in length was purchased from Integrated DNA Technologies (IDT, USA). Low molecular weight (LMW) CS (molecular weight of 190 kDa, 75–85% degree of deacetylation) was purchased from Sigma-Aldrich (Ireland). Glacial acetic acid (99.7% purity) was purchased from R&M Chemicals, UK. Pluronic PF-127 was purchased from Sigma-Aldrich (Missouri, USA). Polyethylene glycol 400 (PEG 400) with the average molecular mass of 380 – 420 g/mol was procured from Merck (Darmstadt, Germany). Distilled water was produced in the laboratory using Water Still Cabinet (Hamilton, United Kingdom).

For cell viability tests, HDFs (passage 2–8) were isolated from human skin samples after obtaining consent from patients. This study was approved by Universiti Kebangsaan Malaysia Research Ethics Committee (UKM 1.5.3.5/244/FF-2015–376). Dulbecco's Modified Eagle's Medium (DMEM) (high glucose) consisting 4.5 g/L D-(+)-Glucose, L Glutamine, phenol red, HEPES, 0.05%-Trypsin/0.53 mM-EDTA solution and sodium pyruvate was obtained from Nacalai Tesque (Kyoto, Japan). AlamarBlue® and LIVE/DEAD® test kits were procured from Invitrogen, USA. Pen-Strep (penicillin/streptomycin) and foetal bovine serum (FBS) were purchased from Gibco (USA) while phosphate buffer saline (PBS) was obtained from Invitrogen, USA.

2.2. Methodology

2.2.1. Preparation of cold water (CLRE) and hot water (HLRE) L. Rhinocerotis extracts

L. rhinocerotis powder was extracted using hot and cold water extraction following a previous method established in our laboratory (Katas et al., 2019). Briefly, powdered sclerotium was boiled in distilled water at a ratio of 1:20 (w/v) at 90–95 °C for 60 min to obtain HLRE. Then, the boiled solution was filtered using Whatman No. 1 filter paper and the residues were re-extracted twice. Meanwhile, for cold water extraction, the mushroom powder dispersed in distilled water (1:2) was continuously stirred at room temperature for 8 h prior to keeping at −20℃ overnight. On the next day, the frozen solution was allowed to melt before stirring continuously for 8 h, followed by keeping at −10 ℃. This process was repeated for three times before the solution was filtered using Whatman No. 1 filter paper. Different cold temperatures are used to extract substances with different solubilities in a low temperature solution. The residues obtained were re-extracted twice, followed by centrifugation at 10 000 rpm for 15 min and freeze-dried using a freeze dryer (ScanVac CoolSafe) at −110℃ until dry powder was obtained. The resulting HLRE and cold CLRE were kept at −20 °C prior to analysis.

2.2.2. Biosynthesis of CS-stabilized AuNPs-CLRE and -HLRE

Biosynthesis was carried out following a previous method by Katas et al. (2019). Briefly, CLRE (0.25 mg/mL) and HLRE (0.06 mg/mL) was mixed with 1 mL 0.1 *M* $HAuCl_4$ solution to produce AuNPs with the desired physical characteristics. Subsequently, 1% w/v LMW CS (dissolved in 1% v/v acetic acid) was added into the AuNPs solution. The CS-stabilized AuNPs were then subjected to sonication (Ultrasonic Cleaner 3510, Branson, Marshall Scientific, USA) for 2 h at 40 Hz. The color change of solution to a stable red-purplish-wine was observed, as an indication of AuNPs formation. The pH of AuNPs solution was adjusted from pH 6.8 to 7.4 by adding 1 *M* sodium hydroxide dropwise. Then, the AuNPs solution was centrifuged at 15000 rpm for 30 min to harvest the AuNPs. The resultant AuNPS-CLRE and -HLRE were freeze dried (Freeze dryer, ScanVac CoolSafe) at −110℃ for 2 days.

2.2.3. Particle size, surface charge and morphology

The mean particle size (Z-average) and surface charge (zeta potential) of AuNPs-CLRE and -HLRE were measured by using Photon Correlation Spectrometry (PCS) and Electrophoretic Light Scattering (ELS), respectively (ZS-90 Zetasizer, Malvern Instruments, Worcestershire, UK). All measurements for particle size were performed at 25 °C and at a detection angle of 90°. The morphology of both AuNPs was analysed using scanning electron microscope (SEM) (Merlin Compact, Zeiss, Magnification 12-2000000x) and transmission electron microscope (TEM) (Tecnai Spiri, FEI, Eindhoven, The Netherlands). Both AuNPs were lyophilized (Freeze dryer, ScanVac CoolSafe) at −110℃ for 2 days prior to SEM analysis. On the other hand, few drops of the AuNPs dispersions (in distilled water) were used for TEM analysis. The samples were placed on the carbon coated copper grids and allowed to evaporate at room temperature (25 ± 2 °C) for 1 min. The excess solution was removed using blotting paper prior to viewing under the TEM. The contrast and brightness of the images were adjusted to optimal values to ensure particles could be viewed clearly.

2.2.4. DsiRNA adsorption

The optimized lyophilized AuNPS-CLRE and -HLRE were suspended in distilled water to produce suspensions of different AuNPs concentrations (0.06, 0.125 and 0.25 mg/mL). Approximately, 1 mL DsiRNA against PGT gene (0.015 μg/mL) was added into 1 mL of each AuNPs-CLRE and -HLRE suspension. The resulting mixture was then incubated at room temperature for 1 h to produce DsiRNA-AuNPs.

2.2.5. DsiRNA entrapment and binding efficiency

The entrapment efficiency (EE) of DsiRNA loaded onto AuNPs was measured using a UV–visible spectrophotometer (UV spectrometer 1800, Shimadzu, Kyoto, Japan). DsiRNA-AuNPs were centrifuged at 10000 rpm for 30 min (Universal 320 R ultracentrifuge, Andreas Hettich GmbH & Co., Germany). The absorbance (A) of supernatant recovered from centrifugation was measured at 260 nm and scanned at 480 mm/min. The DsiRNA entrapment efficiency was calculated using the formula below:

$$\text{DsiRNA EE}\ (\%) = \frac{(\text{Absorbance of DsiRNA added} - \text{Absorbance of DsiRNA in supernatant})}{(\text{Absorbance of DsiRNA added})} \times 100$$

The binding efficiency of DsiRNA onto the AuNPs surfaces was determined using E-Gel™ 4% agarose stained with ethidium bromide (Invitrogen, USA). Naked DsiRNA was used as positive control while 10 bp DNA ladder (Invitrogen, USA) as a size reference. Approximately, 20 μL sample (containing different concentrations of AuNPs-CLRE and AuNPs-HLRE loaded with 15 μg/mL of DsiRNA) were loaded in each well. Electrophoresis were run for 30 min according to E-Gel™ protocol on E-Gel™ Power Snap Electrophoresis Device (Thermofisher Scientific).

2.2.6. Incorporation of DsiRNA-AuNPs into thermoresponsive gels

Approximately, 10 mL of different concentrations of DsiRNA-AuNPs (6, 12 and 25% w/v) was mixed with PF127 (3.75 g). The mixture was magnetically stirred at 200 rpm for 4 h at 4 ± 2 °C and kept at 4 °C overnight. On the next day, 22% w/v of PEG 400 was gradually added into the mixture and stirred at 200 rpm for 4 h at 4 ± 2 °C. The mixture was kept at 4 °C until further analysis.

2.2.7. Characterization of thermoresponsive gels containing DsiRNA-AuNPs

2.2.7.1. Gelation temperature (T_{gel}) measurement. A cold sample of PF 127 formulation (4 °C) was poured into a beaker with a magnetic stirring bar. The beaker was placed on the preheated evaporating dish (100 °C) and maintained at a constant magnetic stirring of 200 rpm. A thermometer was immersed in the cold sample solution to monitor the temperature. The temperature at which the magnetic stirring bar stopped moving was recorded as T_{gel}.

2.2.7.2. Texture profile analysis (TPA). TPA was carried out using a texture analyzer (Brookfield CT-3, United States of America) which was operated in a compression mode. The parameters were set as follows: trigger load at 0.1 N, test speed at 1 mm/s and holding time of 0.15 s. Each gel sample (10 mL) was placed in a glass jar. An analytical probe with disc (38.1 mm diameter) was inserted into the glass jar during each analysis. TexturePro CT V1.5 Build 20 software was used to analyse the results and generate a graph of resultant force (N) against time (s). The hardness, adhesiveness and cohesiveness of the gels were obtained from the plotted graph. Hardness represents the maximal force achieved during the downward movement of the disc, while cohesiveness shows the work required to compress the disc into the gel. Adhesiveness is the work required in the upward movement of disc after compression.

2.2.7.3. Rheology analysis. Rheological profile of the thermoresponsive gels was analysed using a rheometer (Bohlin Gemini, Worcestershire, United Kingdom). Cone and plate geometry at 20 mm diameter and 2° angle was used at 25 °C. The shear rate range was set from 0 to 500 s^{-1}. Small amount of sample was loaded on the plate of the rheometer. Shear rate against shear stress graph was plotted by using Bohlin Software: GEMINI 200 to determine the flow property of gel.

2.2.7.4. In-vitro drug release of active agents. Franz diffusion cells system (PermeGear Inc., Hellertown, USA) was used to determine the *in vitro* DsiRNA and AuNPs release from the gels. Cellulose acetate was used as the membrane and fixed between the donor and the receptor chamber. The diameter of orifice between the donor and receptor was 9 mm with diffusion area of 0.636 cm^2. The receptor chamber (with volume of 5.5 mL) was filled with 5 mL PBS and stabilized for 30 min. The magnetic stirring bar was then added into the receptor containing PBS and the whole system was maintained at 37 ± 2 °C. Gel sample (1 mL) containing DsiRNA-AuNPs was applied on the upper area of cellulose acetate membrane. Sampling was done by taking 1 mL of PBS in the receptor chamber at the pre-determined time points (0, 1, 2, 3, 4, 5, 6, 7, and 8 h). Then, 1 mL of taken sample was immediately refilled with fresh PBS. The absorbance of samples was analysed using UV–Vis spectrophotometer at 260 nm for DsiRNA while 400 to 600 nm for AuNPs. The cumulative amount/frequency of DsiRNA and AuNPs over the surface area (μg/cm^2) of membrane was calculated and plotted against time (h).

2.2.8. In-vitro safety and efficacy testing

2.2.8.1. Cell morphological test. Briefly, 2.5 × 10^4 HDFs supplemented with DMEM containing 10% FBS and 1% Pen-Strep were seeded in 48-well plates and incubated for 24 h at 37 °C in an incubator supplied with 5% CO_2. Then, the cells were exposed to different concentrations of AuNPs (0.06, 0.125, 0.25, 0.5, 1, 2, 3 and 4 mg/mL) at a nanocomposite to growth media ratio of 1:1 for 24 h. The cells in each well were exposed to approximately 30, 60, 125, 250, 500, 100, 150 and 200 μg AuNPs for 0.06, 0.125, 0.25, 0.5, 1, 2, 3 and 4 mg/mL AuNPs, respectively. Later, the number and morphological of HDFs were observed and captured using an inverted phase contrast microscope (Olympus CK40, Tokyo, Japan). Then, the cells were washed with PBS solution and replaced with fresh DMEM prior to incubation at 37 °C and supplied with 5% CO_2. The steps were repeated for the cell morphological test at 48 and 72 h.

2.2.8.2. Cell viability test. Approximately, 1 × 10^4 of HDFs was seeded in 96-well plates and the cells were supplemented with DMEM containing 10% FBS and 1% pen-strep. The cells were incubated at 37 °C in an incubator supplied with 5% CO_2 for 24 h. Subsequently, the cells were exposed to 100 μL DsiRNA-AuNPs (0.06,

0.125, 0.25, 0.5 and 1 mg/mL) for 24, 48 and 72 h. The cells in each well were approximately exposed to 6, 12.5, 25, 50 and 100 μg AuNPs for 0.06, 0.125, 0.25, 0.5 and 1 mg/mL DsiRNA-AuNPs, respectively. After incubation, the media was replaced with fresh growth media, followed by the addition of 10% AlamarBlue® solution and the cells were incubated for 4 h. The absorbance of cell suspensions was measured at 570 nm using a microplate reader (Bio Tek PowerWave XS, US) after the solution was transferred to a new plate. The same procedure was repeated at 48 and 72 h of treatment. The amount of cell viability was calculated as the formula below:

$$\text{Percent of cell viability}\,(\%) = \frac{(\text{Absorbance of sample})}{(\text{Absorbance of control})} \times 100$$

2.2.8.3. Cell viability determination via live and dead assays. In this experiment, HDFs (2.5×10^4) in DMEM were seeded in 48-well plates and incubated for 24 h in an incubator at 37 °C, supplied with 5% CO_2. After 24 h, the cells were exposed to DsiRNA-AuNPs (0.06, 0.125 and 0.25 mg/mL) for 48 h. Then, the cells were stained with LIVE/DEAD® Viability/Cytotoxicity Kit for mammalian cells (Invitrogen USA) according to the manufacturer's protocol. The cells were washed with sterilized PBS and then incubated with the working solution (2 μm calcein AM and 4 μm ethidium homodimer 1-red (EthD-1) in sterilized PBS) for 30 min. The cells were then viewed under a fluorescence microscope (Nikon A1R, Japan).

2.2.8.4. Cell proliferation. Pluronic gels containing different concentrations of DsiRNA-AuNPs (6, 12.5 and 25% w/v, F6-F11) were placed in 96-well plates. The plates were sterilized by exposing to UV light for 5 min prior to starting the experiment. HDFs (1×10^4) were then seeded on top of the gels as previously reported (Loh et al., 2018). The cells treated with DMEM was used as positive control while blank wells (without cells) as negative control. After 24 h, the cells were washed with sterilized PBS solution and replenished with fresh growth media. AlamarBlue® (10%) was added into each well and incubated for 4 h. Then, the solution was transferred to new 96-well plates prior to the absorbance measurement using a spectrophotometer (Bio-Tek, PowerWave XS, USA) at 570 and 600 nm. The cells in the plates were washed with sterilized PBS, replaced with fresh medium and allowed to grow in an incubator at 37 °C supplied with 5% CO_2. The procedure was repeated at 48 h incubation. The percent reduction of AlamarBlue® was calculated as below:

$$\text{Percent of reduction}\,(\%) = \frac{[(\varepsilon OX)\lambda 2A\lambda 1 - (\varepsilon OX)\lambda 1A\lambda 2]}{\left[(\varepsilon RED)\lambda 1A'\lambda 2 - (\varepsilon RED)\lambda 2A'\lambda 1\right]} X100$$

Where, (εOX)λ2 = 117216; (εOX)λ1 = 80586; (εRED)λ1 = 1556 77; (εRED)λ2 = 14652; Aλ1 and Aλ2 was the observed absorbance reading for test well at 570 and 600 nm.

2.2.8.5. Cell migration assay. In migration assay, 5×10^4 cells/well of HDFs were seeded in 24-well plates. The cells were incubated in an incubator under condition of 5% CO_2 and at 37 °C until fully confluent or monolayer of cells was formed. Once confluent, the cells were washed with PBS solution. A scratch was made by using 10 μL micropipette tip in the middle of each well. The cells were washed with DMEM to remove cell debris from the scratching. The gel and growth media at a ratio of 1:1 were slowly added into each well. Migration of cells in each well was visualized using an inverted phase contrast microscope (Olympus CK30, Japan) connected to a digital camera (Xcam-α) comprised of DigiAcquis version 2.0 software. Series of a point were set and the pictures within the area of the set point were captured at 0, 24 and 48 h.

2.2.9. Statistical analysis

All data are presented as mean ± SD. The data were analysed using one-way ANOVA and two-way ANOVA followed by post-hoc Bonferroni test using GraphPad Prism software (5th version). The differences among the groups tested were considered significant if $p < 0.05$.

3. Results and discussion

3.1. Formation and physical characteristics of CS-AuNPs

Phytochemical analysis using LC-MS revealed that CLRE and HLRE contain oligosaccharides, polysaccharides, fatty acids and phenols (Katas et al., 2019). A high carbohydrate content was also reported for the extracts of *L. rhinocerotis* sclerotium (Yap et al., 2014), a rich source of reducing agents. The formation of both AuNPs was indicated by the change of solution color from yellow to ruby-red violet after 90 min and the formation was confirmed by the absorption band around 523–544 nm which is a typical Plasmon resonance band for AuNPs, suggesting the formation of AuNPs as determined by UV spectrometry (Ismail et al., in press; Katas et al., 2019). The appearance of violet-red colour is an evident of AuNPs formation in a reaction (Nayak, 2014). In this study, AuNPs were synthesized using 0.25 and 0.06 mg/mL of CLRE and HLRE, respectively due to the optimal physical characteristics of the AuNPs produced as well as their high antibacterial activity against gram positive and negative bacteria as reported previously (Katas et al., 2019). The particle size of AuNPs-CLRE was 208 ± 36 nm while smaller particles were obtained for AuNPs-HLRE (190 ± 33) with polydispersity index (PDI) of 0.4, indicating intermediate particle size distribution. Both AuNPs possess positive surface charges with lower value for AuNPs-CLRE (+30 ± 22 m V) than AuNPs-HLRE (+45 ± 8 mV). CS capping attributed to the positive charges of AuNPs, resulting in a stable solution of nanoparticles (Czechowska-Biskup et al., 2015, Katas et al., 2019). SEM micrographs show that the average particle size of AuNPs-CLRE and -HLRE was in the range of 110–140 nm and 50–150 nm, respectively. The particles were spherical in shape with some degree of aggregation. Contrarily, the average particle size of AuNPs-CLRE and -HLRE was approximately 15–17 nm and 20–22 nm, respectively as determined by TEM. Both AuNPs were mostly spherical particles with the appearance of some triangular particles as well (Fig. 1**(a)**). Morphological analysis of AuNPs using SEM revealed the formation of aggregates to a certain extent, explaining the larger particles of AuNPs measured by PCS and SEM as compared to TEM. Freeze drying might attribute to the aggregate formation as TEM was used to analyze non-lyophilized AuNPs. The small size of these AuNPs (nano-sized range) would provide high surface area to volume ratio, allowing high load of active agent (DsiRNA) on the surface of the nanocomposites.

3.2. DsiRNA EE and binding efficacy

DsiRNA against PGT gene that poses negative charges was adsorbed onto the surfaces of positively charged AuNPs via electrostatic interactions to promote vascularization and subsequently, the healing process of diabetic wound. Three concentrations of AuNPs-CLRE and -HLRE (0.06, 0.125 and 0.25 mg/mL) were loaded with DsiRNA on their surfaces owing to their high antibacterial activity against *Staphylococcus aureus* (gram positive bacteria), *Pseudomonas aeruginosa* and *Escherichia coli* (gram negative bacteria) as studied previously (Katas et al., 2019). The EE of DsiRNA adsorbed onto different concentrations of AuNPs is shown in Table 1. All the AuNPs were able to load DsiRNA with high EE (more than 80%). The high EE provides an early indication that

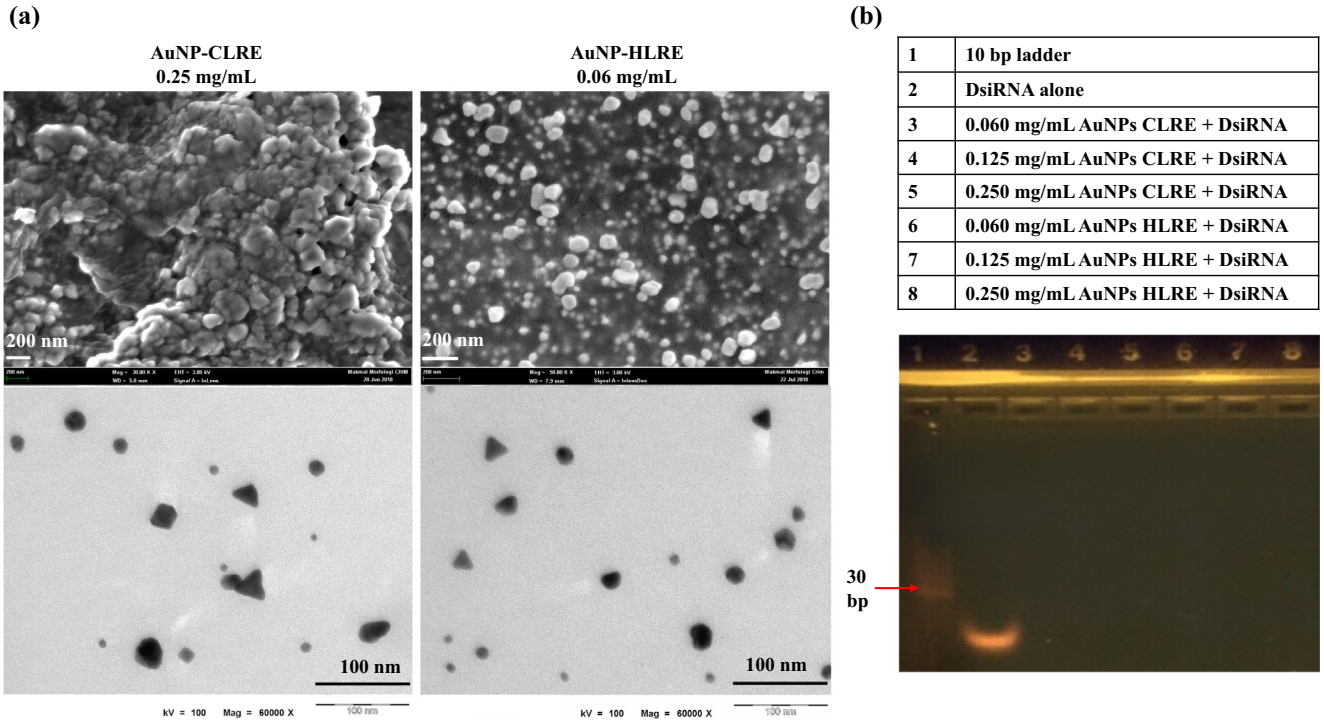

Fig. 1. (a) Morphology of AuNPs under SEM (above) and TEM (below); (b) Binding efficiency of DsiRNA onto different types AuNPs and at various concentrations of AuNPs.

Table 1
The effect of type and concentration of AuNPs on DsiRNA EE, n = 3.

Type of AuNPs	Concentration of DsiRNA-AuNPs, mg/mL	EE (%)
AuNPs-CLRE	0.06	85 ± 6
	0.125	85 ± 9
	0.25	88 ± 9
AuNPs-HLRE	0.06	83 ± 2
	0.125	83 ± 11
	0.25	84 ± 3

AuNPs were able to potentially deliver active dose efficiently to the target site (Katas et al., 2017). Furthermore, the type and concentration of AuNPs had no significant impact on the EE of DsiRNA. On the other hand, the absence of a trailing band of DsiRNA after being electrophored indicated the strong binding between DsiRNA and AuNPs (Fig. 1**(b)**). AuNPs were trapped in the well of gel owing to their large size, precluding the migration across the gel matrix. This finding demonstrated that the AuNPs would be able to carry and protect DsiRNA, indicating the potential of these AuNPs in delivering DsiRNA to diabetic wound.

3.3. T_{gel} of formulation

The optimal T_{gel} is extremely crucial to develop a topical formulation with fast protective effect for wounds. Thermoreversible gel for topical delivery should exist as liquid or solution at room temperature and undergo gelation to form a stable depot at skin/body temperature (Rarokar et al., 2018). The molecules of the gel exhibit a zigzag conformation which transform into a close-packed meander arrangement, forming a viscous gel as the temperature rises (Kramaric et al., 1992). The blank gel composed of 25% w/v PF127 (F1) was gelled at the temperature below 25 °C (Table 2). A gel formulation consisting a concentration of 25% PF127 was reported to obtain hydrogels with the transition temperature approximately at 20 °C with good texture and rheology (Geng et al., 2011). PF127 has flowing properties (sol phase) at or below room temperature and rapidly turns into the semisolid rigid mass (gel phase) between room and skin/body temperature. The temperature of PF127 can be disrupted depending on the concentration of PF127 and additives used (Akash et al., 2014). To achieve the desired T_{gel} for the skin delivery (~32–36 °C) (Ban et al., 2017), the gelation property of PF127 was altered with the addition

Table 2
T_{gel} of PF127 formulations with different concentrations of PEG400, AuNPs-CLRE and AuNPs-HLRE, n = 3.

Formulation code	PF127, % w/v	PEG 400, %w/w	DsiRNA-AuNPs (CLRE), mg/mL	DsiRNA-AuNPs (HLRE), mg/mL	T_{gel} (°C)
F1 (blank)	25	–	–	–	24 ± 1
F2	25	5	–	–	27 ± 1
F3	25	10	–	–	30 ± 1
F4	25	15	–	–	33 ± 1
F5	25	22	–	–	37 ± 1
F6	25	22	0.060	–	28 ± 1
F7	25	22	0.125	–	26 ± 1
F8	25	22	0.250	–	27 ± 1
F9	25	22	–	0.060	32 ± 1
F10	25	22	–	0.125	29 ± 1
F11	25	22	–	0.250	27 ± 0

of co-polymers as they would interfere with micellization of the polymer, resulting in increased T_{gel}.

In present study, PEG 400 was added into the gel to achieve targeted T_{gel} of around skin/body temperature. PEG 400 is a water-soluble polymer synthesized from ethylene oxide, comprising of a repeating unit of -(O-CH_2-CH_2)- (Hutanu et al., 2014). PEG 400 was used to increase the T_{gel} of PF127 due to its ability in forming stable micelle clusters with PF127. PEG 400 is also equipped with the capability as a wound sealing and healing (Petkova-Olsson et al., 2017), making it a good candidate as a co-polymer. Different concentrations of PEG 400 were added into 25% w/v PF127 (F2-F5) as shown in Table 2. The T_{gel} of PF127 increased from 27 ± 1 °C to 37 ± 1 °C by increasing the concentration of PEG 400 from 5% to 22% w/w. Pisal et al., (2004) reported similar findings as PEG 400 facilitated the increase of PF127 T_{gel} and the effect was influenced by the added PEG concentration.

The hydrophilic end chains of PF127 comprise the same polyethylene oxide (PEO) chains as presented in PEG 400. The binding of ester group to these chains promote dehydration of hydrophobic polypropylene oxide (PPO) block, thus, causing an increase in the entanglement of the adjacent micelles, resulting in higher T_{gel} with increasing the PEG 400 concentration (Agrawal & Maheshwari 2014). Based on the obtained results (Table 2), 25% PF127 with the addition of 22% PEG 400 (F5) was selected for further development as the formulation had the target T_{gel}. Therefore, the formulation F5 was selected for the incorporation with DsiRNA-AuNPs (AuNPs-CLRE and -HLRE) at the concentrations that exhibited high antibacterial activity (0.06, 0.125 and 0.25 mg/mL, represented as F6-F11, respectively) as reported by our research group previously (Katas et al. 2019).

Interestingly, the T_{gel} decreased abruptly in the range of 26 °C ± 1 – 32 °C ± 1 when DsiRNA-AuNPs was added into the formulation ($p < 0.05$, one-way ANOVA, Bonferroni's post hoc analysis). The T_{gel} reduced as the concentration of AuNPs-CLRE and -HLRE was increased, probably due to the capping effect of CS. The addition of polymers such as CS, linoleic acid, hyaluronic acid, acrylic acid and alginate as crosslinkers for PF127 gel, significantly reduces the concentration of PF127 required to achieve critical gelation concentration for sol–gel transition phase (Akash et al., 2014). However, T_{gel} of the gels containing DsiRNA-AuNPs was still in the acceptable range for skin delivery.

3.4. TPA of formulation

Concentration of gelling agent in a formulation is an important contributing factor of the gel mechanical properties. Properties such as good skin spreadability, easy removal of product from the container, acceptable viscosity and good bioadhesion are required in a topical formulation intended for wound healing (Jones et al., 1997; Hurler et al. 2012). Hardness indicates the applicability of gel at the desired site. Meanwhile, cohesiveness provides useful information regarding the easiness of gel removal from the container and its spreadability at the application site. Low values of both are required for easy removal of gel from the container and application on the skin epithelia (Baloglu et al., 2011). In comparison to the blank gel of PF127 alone (F1), the addition of PEG 400 lowered the hardness and cohesiveness and both values were further reduced with increasing the PEG 400 concentration from 5% to 22% (F2 – F5) (Fig. 2).

Adhesiveness is defined as the work required in overcoming the attractive forces between the sample and probe surfaces, occurs when cohesive bonds are broken (Jones et al., 1996). The greater the adhesiveness value, the greater the adhesion of gel at the skin epithelia, contributing to prolong retention time (Cevher et al., 2008). Despite the addition of PEG 400 lower the adhesiveness of PF127 gels, F5 demonstrated the highest adhesiveness ($p < 0.05$,

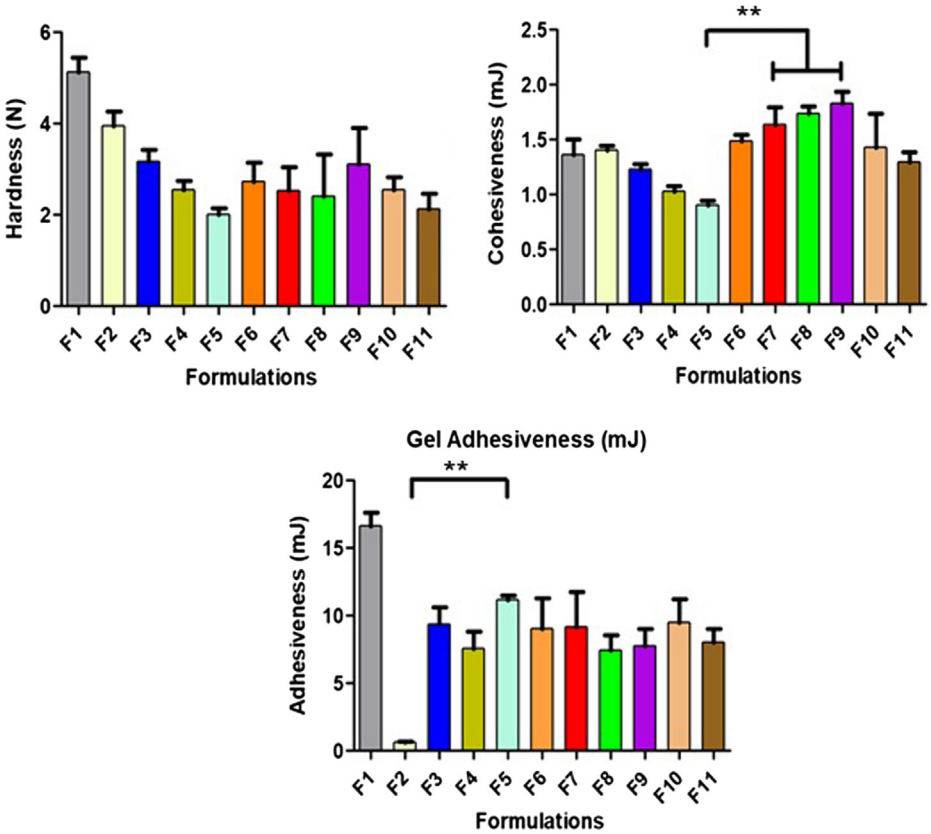

Fig. 2. TPA of the thermoresponsive gels consisting PF 127, PEG 400 and DsiRNA-AuNPs, n = 3. *- indicates significant different.

two-way ANOVA, Bonferroni's post hoc analysis). Therefore, F5 was selected to incorporate with DsiRNA-AuNPs as it also exhibited the lowest hardness and cohesiveness with the target T_{gel}.

The combination of F5 with different concentrations of DsiRNA-AuNPs (F6-F11) did not affect the hardness. Similar to hardness, the cohesiveness was not influenced by the addition of DsiRNA-AuNPs as only F7 was significantly different from F5 statistically ($p < 0.05$, one-way ANOVA, Bonferroni's post hoc analysis) although the gel cohesiveness increased as higher concentrations of AuNPs-CLRE (F6-F8) were added and the opposite relationship was observed for AuNPs-HLRE (F9-F11). The cohesiveness values for all the gels containing DsiRNA-AuNPs were close to unity, indicating the absence of breakage in the gel structure and thus, easy handling of the formulation could be expected (Calixto et al., 2015). Moreover, all the gels containing DsiRNA-AuNPs had comparable adhesiveness as F5, indicating that the addition of AuNPs did not affect this property.

3.5. Rheology of formulations

Rheological profile of formulation was analysed to predict *in-situ* behaviour of gel formulation at around the skin/body temperature (Baloglu et al., 2011). All the formulations (F1-F11) exhibited non-Newtonian linear curve (shear-thinning) as illustrated in Fig. 3**(a-b)**. The gels were predicted to manifest pseudo-plastic or non-Newtonian characteristics due to its thermo-sensitive property (Katas et al., 2017). A non-Newtonian fluid is characterised by the flow curve (shear rate against shear stress) and it is a non-linear or does not pass through the origin point. Regardless of PEG concentration and the addition of DsiRNA-AuNPs, a decrease in viscosity was observed for all the gels with increasing the shear rate. The decrease in viscosity was expected due to the disruption of molecule alignments of the polymer under the application of shear stress, causing the molecules to flow easily with a gradual decrease in viscosity (Al-Shammari et al., 2011). Fig. 3**(c)** presents the apparent viscosity of the thermoresponsive gels that gradually reduced with the increasing concentrations of PEG 400 at 25 °C ($p < 0.05$, one-way ANOVA, Bonferroni's post hoc analysis). This was expected as PEG 400 disrupted polymeric structure of the tri-blocks PF127 polymer (Bentley et al., 1999). The addition of DsiRNA-AuNPs further lowered the viscosity of the gels (F6-F11) ($p < 0.05$, one-way ANOVA, Bonferroni's post hoc analysis), as the AuNPs might also disrupt the structure of PF 127.

3.6. In-vitro release of active agents

Franz diffusion cell was used to analyze the release of active agents from the optimal thermoresponsive gels containing DsiRNA loaded onto different concentrations (0.06, 0.125 and 0.25 mg/mL) of AuNPs-CLRE (F6-F8) and AuNPs-HLRE (F9-F11). From the results obtained, the release of AuNPs-CLRE and -HLRE were similar, regardless of their concentration (Fig. 4**(a)**). Generally, the amount of AuNPs released showed an increase up to 7 h, followed by a decrease in AuNPs release. The finding was differing from a previous report that higher permeation of AuNPs was observed as their concentration was increased (Filon et al., 2011). The gel could be the barrier that acted as the limiting factor for drug release because it could be dictated by the diffusion of AuNPs across the gel. The AuNPs release was affected by PF127 as a complete release was achieved for AuNPs incorporated in PF127 gel within 5 h (Arafa

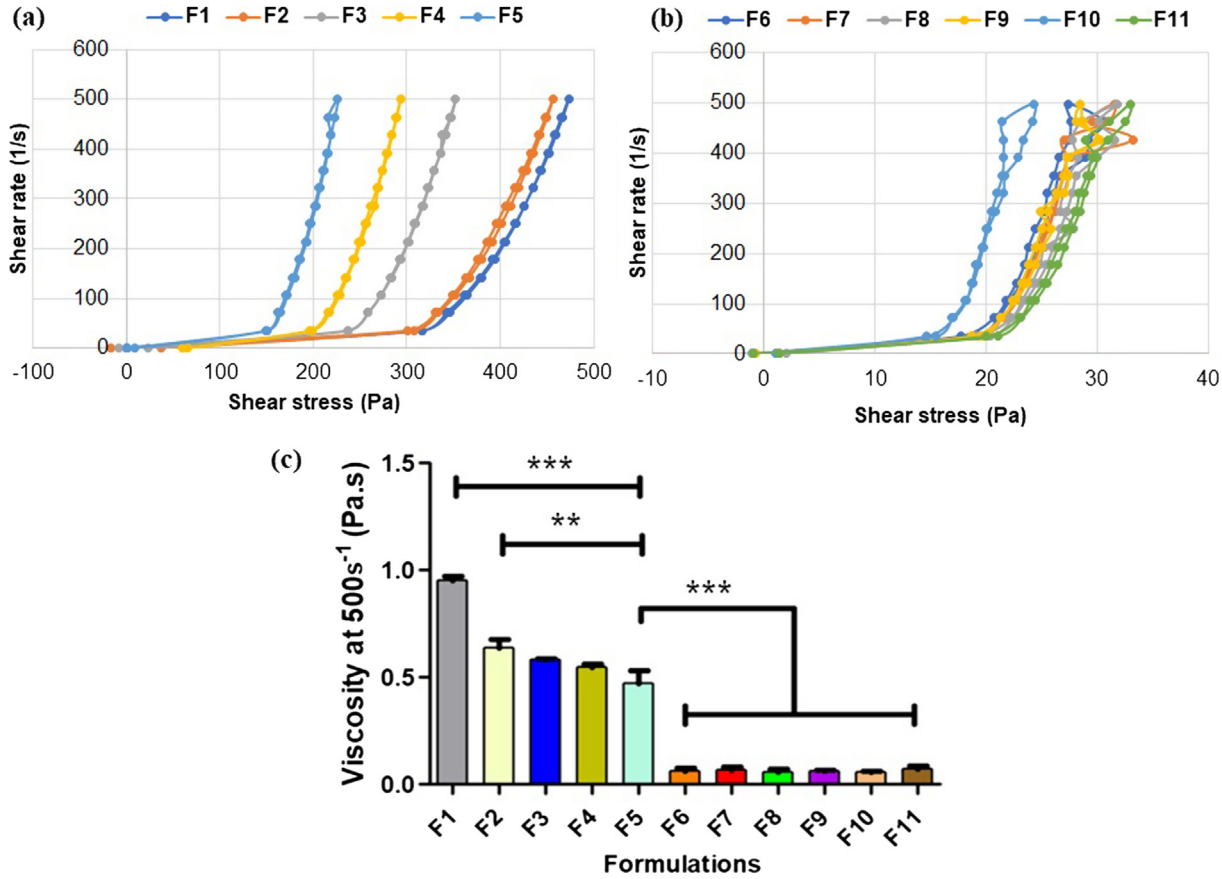

Fig. 3. Rheological profiles of different thermoresponsive gel formulations for (a) F1-F5 and (b) F6-F11 as well as (c) their apparent viscosity at 25 °C, n = 3. *- indicates significant different.

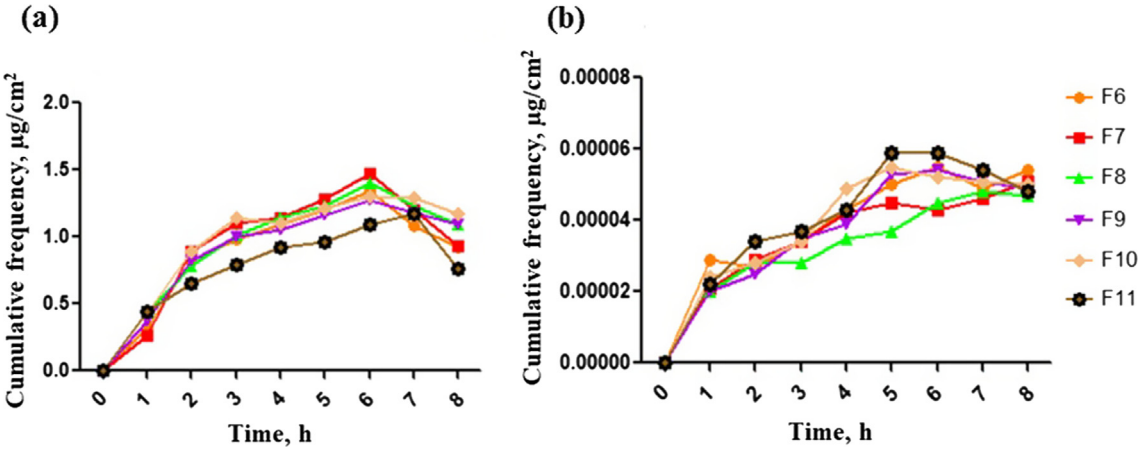

Fig. 4. *In-vitro* drug release of AuNPs (a) and DsiRNA (b) from thermoresponsive gels (F6-F11), n = 3.

et al., 2018) and diffusion through the polymeric matrices was suggested as the release mechanism (Machado et al., 2013).

The particle size of AuNPs also plays an important role in the release of loaded drug, owing to higher surface area to volume ratio of smaller particles. Despite both AuNPs had different particle size, the release of DsiRNA was similar to one another due to a small difference for their size. It should be also noted that the same concentration of DsiRNA was adsorbed onto the surface of different concentrations AuNPs, explaining similar amount of DsiRNA was being released. Moreover, different concentrations AuNPs had similar EE and binding efficiency, attributed to the same release pattern. CS nanoparticles with a low EE usually release DsiRNA more rapidly due to the weak intermolecular linkages between DsiRNA and CS than the ones with higher EE (Katas et al., 2017). All the gels showed an increase in the release of DsiRNA within the first five hours, followed by a more constant release (Fig. 4**(b)**).

3.7. In vitro safety and efficacy

3.7.1. Cell morphology and cytotoxicity effects

The safety use of AuNPs was first studied prior to adsorption with DsiRNA and incorporated into the thermoresponsive gel via cell morphological and cell viability assays. These tests were conducted to ensure the concentration of AuNPs used for further development is safe and biocompatible with cells. The toxicity is commonly related to inorganic materials such as AuNPs when exposed to high concentrations. Moreover, metal nanoparticles can penetrate skin through hair follicles and reach to the deeper skin of basal and spinous layers that could potentially damage the skin (De Matteis, 2017). Cell morphological assay is a qualitative test that examines the size and shape of HDFs after being exposed to different concentrations AuNPs-CLRE and -HLRE. By determining the non-toxic concentration range of AuNPs to HDFs, this assay acted as a pre-analysis before conducting cytotoxicity and proliferation assays. As shown in Fig. 5**(a)**, HDFs remained their spindle shape with the appearance of lamellipodia and filopodia protrusions. The cells continued to grow and proliferate after being exposed to both types of AuNPs at a concentration from 0.06 to 1 mg/mL for 72 h. At higher AuNPs concentration (2 mg/mL), HDFs were not viable anymore and appeared as rounded cells. Unlike AuNPs-CLRE, HDFs were viable and growing even though the cells were exposed to AuNPs-HLRE at the same high concentration. This indicated that AuNPs-HLRE were less toxic than AuNPs-CLRE. However, at very high AuNPs concentrations (3 and 4 mg/mL), the cells were all not viable anymore with obvious change in the cell morphology after 24 h of incubation for both AuNP types. The finding demonstrated that the toxicity of AuNPs was concentration dependent (de Vierra et al., 2017; Steckiewicz et al., 2019). The safety evaluation of AuNPs was further carried out by conducting cell viability assay, a form of colorimetric assay that determines and estimates the cytotoxicity of AuNPs (Mahmood et al., 2019). The toxicity of AuNPs depends on their physicochemical properties including particle size, surface charge and chemistry of their surface (Darweesh et al., 2019).

Based on the results of cell morphology assay, AuNPs concentration from 0.06 to 1 mg/mL were tested in cell viability assay. The cell viability of AuNPs-CLRE and -HLRE is shown in Fig. 5**(b)**. Similar to the results of cell morphological assay, higher AuNPs concentrations reduced the cell viability of HDFs more than lower concentrations ($p < 0.01$, two-way ANOVA, Bonferroni's post hoc analysis). This effect was more prominent for AuNPs-CLRE than -HLRE. The cytotoxicity of AuNPs has been reported to be concentration dependent, regardless of the extract used as reducing agent in the synthesis of AuNPs. For example, the cytotoxicity of AuNPs synthesized from pyomelanin purified from *Yarrowia lipolytica* (a type of yeast) also increased as the AuNPs concentration was increased from 5 to 160 µg/mL (Tahar et al., 2019). Moreover, the toxic effect of AuNPs-CLRE and -HLRE could be transient as the HDFs viability increased after prolong incubation, at 48 and 72 h except for high concentrations of AuNPs-HLRE as the cell viability slightly decreased from 68% ± 18 to 59% ± 12 and 74% ± 21 to 65% ± 9 for 0.5 and 1 mg/mL AuNPs, respectively.

Despite that, the cell viability of AuNPs at a concentration from 0.06 to 0.25 mg/mL was comparable to positive control (non-treated cells), indicating the non-toxicity of AuNPs at these concentrations and therefore, the concentrations were further tested in *Live and Dead* assay. The assay is a qualitative test for further confirming the non-toxicity of AuNPs at the selected concentration range. The live cells appear as green while dead cells appear as red. Based on Fig. 5**(c)**, more live cells were observed (green) compared to dead cells (red), indicating high cell viability of HDFs after exposing to AuNPs for 48 h.

3.7.2. Cell proliferation assay

Cell proliferation assay was carried out for determining any change in cell proportion, the dividing cell. In this assay, DsiRNA-AuNPs incorporated into the thermoresponsive gels were tested (F6-F11) by seeding HDFs on top of the gels. Based on the results presented in Fig. 6**(a)**, all the gels enhanced the HDFs proliferation as the percent of resazurin reduction to resofurin increased from 24 to 48 h, indicating the growth and proliferation of HDFs. The

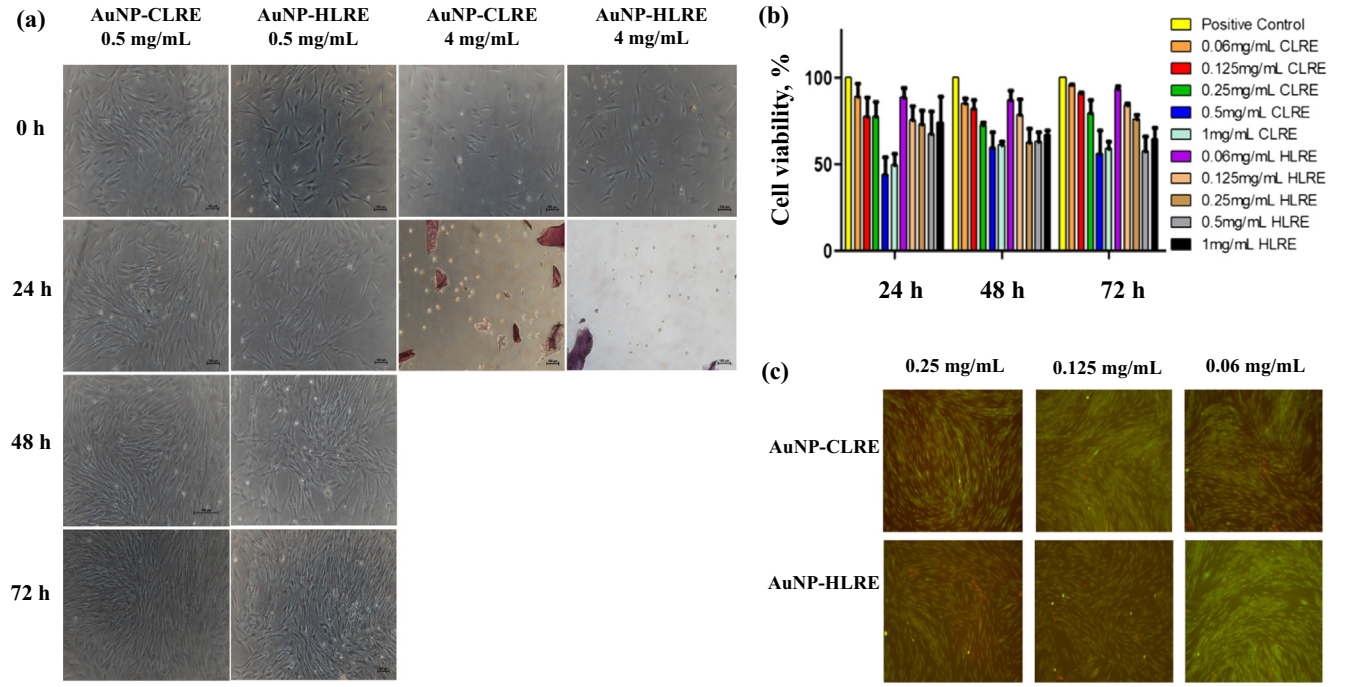

Fig. 5. (a) Cell morphology of HDFs exposed to AuNPs-CLRE and -HLRE; (b) percent of cell viability of HDFs exposed to different concentrations of DsiRNA-AuNPs for 24, 48 and 72 h (n = 3) and (c) Fluorescent micrographs of HDFs exposed to DsiRNA-AuNPs for 48 h and analysed via *Live and Dead* assay.

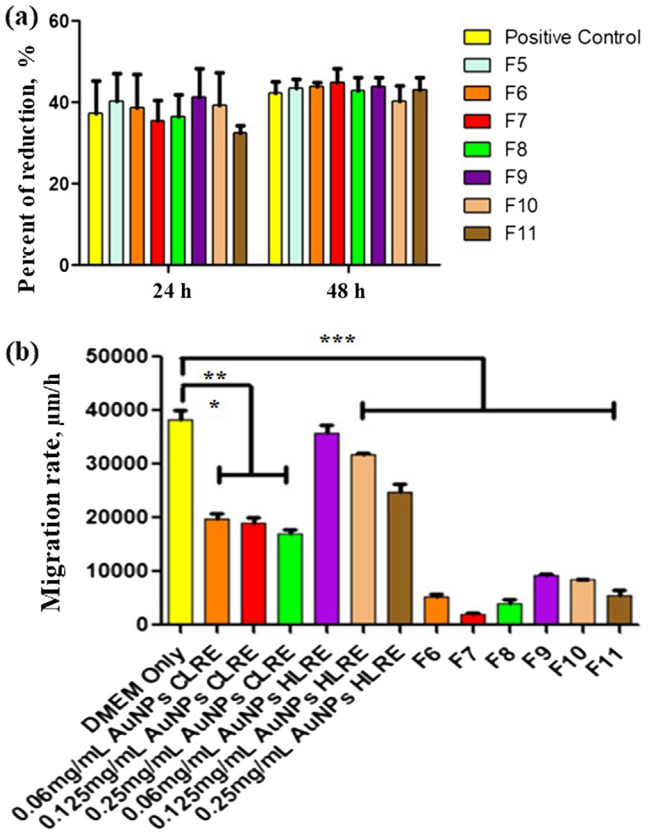

Fig. 6. (a) Percent of resazurin reduction for thermoresponsive gels containing different concentrations of DsiRNA-loaded AuNPs-CLRE and -HLRE (F6-F11) and (b) Migration rate of HDFs exposed to the thermoresponsive gels containing DsiRNA-AuNPs, n = 3. *- indicates significant different.

proliferation was also found to be unaffected by different types and concentrations of AuNPs.

The ability of AuNPs to carry active agents for wound healing were reported previously. For example, cryopreserved human fibroblast cells vectorized by AuNPs synthesized from a chemical reduction agent (citrate solution) accelerated wound healing. The proposed mechanisms of wound healing include the enhancement of cell proliferation and subsequent regulation of collagen synthesis/degradation as well as alteration of type I and III collagen composition at the wound site (Volkova et al., 2016). AuNPs were also used to deliver basic fibroblast growth factor (bFGF) and the nanocomposites were shown to enhance angiogenesis and fibroblast proliferation and thus, promoting rapid wound closure without causing toxicity (Marza et al., 2019).

3.7.3. In vitro cell migration assay

The *in vitro* wound scratch assay is an economical, easy and well-developed method to study cell migration from the wound edges into the cell-free area (Grada et al., 2017). Therefore, the assay was used to determine the wound healing efficacy of DsiRNA-AuNPs and those incorporated into the thermoresponsive gels. In this experiment, HDFs promoted the cell migration and closed the wound gap after exposing to DsiRNA-AuNPs (Figs. 6**(b) and** 7). HDFs exposed to DMEM only (positive control) migrated and close the wound gap within 17 h, exhibited the highest migration rate (38358 ± 2494 μm/h). DsiRNA loaded onto AuNPs-HLRE (the range of migration rate of 24821 ± 1943 to 35842 ± 215 μm/h) had higher migration rate than AuNPs-CLRE (17065 ± 1116–19 817 ± 1321 μm/h) and the earlier type could close the gap within 17 h while 24 h for the latter type. The effect was also affected by the concentration of AuNPs, the greater the concentration, the lower the migration rate of HDFs observed. The findings were differed from chemically synthesized AuNPs (cat. no., 752584, at 0.1, 1 and 10 μg/mL) that reduced fibroblast migration (Viera., 2017).

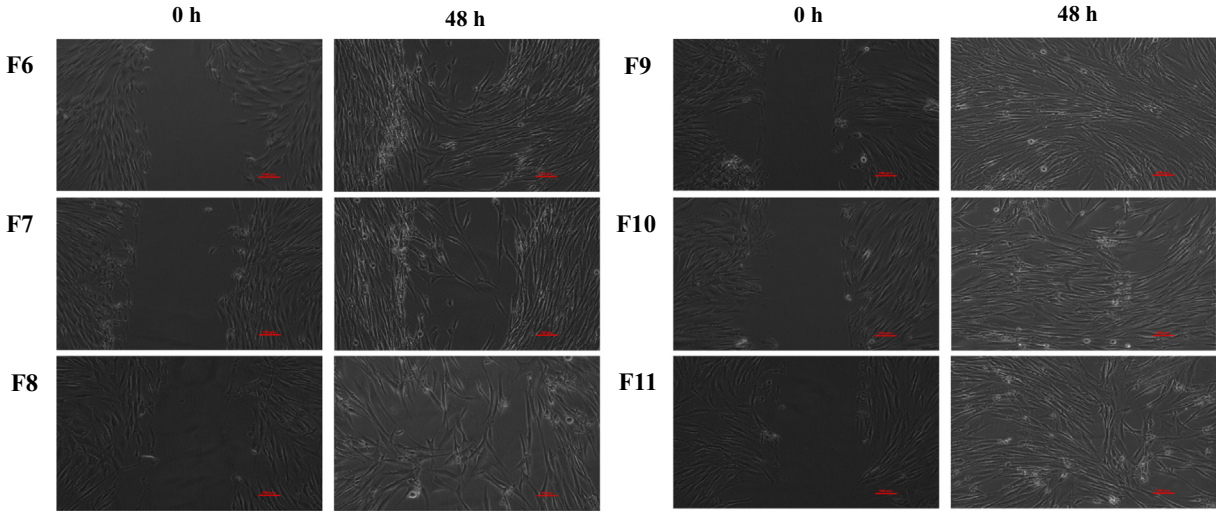

Fig. 7. Wound scratch assay for thermoresponsive gels containing different concentrations of DsiRNA-AuNPs at 48 h (F6-F11). Scale bar represents 100 μm.

PEGylated hollow AuNPs was also reported to affect the migration of mesenchymal stem cells but had no obvious effect on fibroblasts (Encabo-Bersoza et al., 2017), indicating the effect could be influenced by several factors, including the composition of nanocomposites and cell types.

When incorporating DsiRNA-AuNPs into the thermoresponsive gels (F6-F11) and exposed to HDFs, lower migration rate than DsiRNA-AuNPs was observed. Despite the gels containing DsiRNA loaded on AuNPs-HLRE (5594 ± 1514–9390 ± 380 μm/h) had higher migration rate than AuNPs-CLRE (1934 ± 488–5300 ± 770 μm/h) but, they were not significantly different statistically, indicating that the AuNPs type had lesser effect on the cell migration when incorporated into the gel. Nevertheless, the concentration of AuNPs still affected the migration rate after incorporated into the gel as increasing the AuNPs concentration resulted in lower migration rate of HDFs ($p < 0.05$, one-way ANOVA, Bonferroni's post hoc analysis). The gel containing DsiRNA-loaded onto AuNPs-HLRE at 0.06 mg/mL (F9) was the only formulation to achieve full closure of the wound gap within 48 h (Fig. 7) and the rate was comparable to positive control (DMEM only, the highest migration rate), showing the potential of this formulation as wound dressing for diabetic patients. Taken together DsiRNA-AuNPs were shown to accelerate wound healing due to higher survival rate of HDFs than the control as determined in cell viability and proliferation assays. In general, with an exception of F9, the incorporation of the nanocomposites into the thermoresponsive gels had shown to slower the healing rate, probably due to the gel that acted as an additional barrier to the release of DsiRNA and AuNPs at the site of action. Therefore, they may be suitable for sustained release delivery for wound treatment.

4. Conclusions

Dual-action nanocomposites consisting DsiRNA and AuNPs were successfully developed with high EE, suitable as a healing agent for diabetic wound treatment. DsiRNA-AuNPs were also incorporated into thermoresponsive gel made of PF 127 and PEG 400 as a wound dressing that gelled at body temperature with good spreadability and adhesiveness for topical applications. Both nanocomposites and those incorporated into thermoresponsive gels were relatively non-toxic on HDFs and enhanced the cell migration. Taken together, the gels could be the next medicated wound dressing for treating diabetic wounds. The findings of this study would also warrant further pre-clinical studies in animal models for safety and efficacy of the dressings.

Acknowledgement

This study was supported financially by research grants from Universiti Kebangsaan Malaysia (*Geran Universiti Penyelidikan* (GUP-2019-004) and *Arus Perdana* (AP-2017-008/3).

References

Akash, M.S.H., Rehman, K., Chen, S., 2014. Pluronic F127-Based Thermosensitive Gels for Delivery of Therapeutic Proteins and Peptides. Polym. Rev. 54, 573–597. https://doi.org/10.1080/15583724.2014.927885.

Al-Shammari, B., Al-Fariss, T., Al-Sewailm, F., Elleithy, R., 2011. The effect of polymer concentration and temperature on the rheological behavior of metallocene linear low density polyethylene (mLLDPE) solutions. J. King Saud Univ. Sci. 9–14. https://doi.org/10.1016/j.jksues.2010.07.001.

Agrawal, A., Maheshwari, R., 2014. Formulation Development and Evaluation of in situ Nasal Gel of Poorly Water Soluble Drug Using Mixed Solvency Concept. Asian J. Pharm. 5, 131–140 https://doi.org/10.22377/ajp.v5i3.98.

Arafa, M.G., El-Kased, R.F., Elmazar, M.M., 2018. Thermoresponsive gels containing gold nanoparticles as smart antibacterial and wound healing agents. Sci. Rep. 8, 13674. https://doi.org/10.1038/s41598-018-31895-4.

Baloglu, E., Karavana, S.Y., Senyigit, Z.A., Guneri, T., 2011. Rheological and mechanical properties of poloxamer mixtures as a mucoadhesive gel base. Pharm. Dev. Technol. 16, 627–636. https://doi.org/10.3109/10837450.2010.508074.

Ban, E., Park, M., Jeong, S., Kwon, T., Kim, E.-H., Jung, K., Kim, A., 2017. Poloxamer-Based Thermoreversible Gel for Topical Delivery of Emodin: Influence of P407 and P188 on Solubility of Emodin and Its Application in Cellular Activity Screening. Molecules 22, 246. https://doi.org/10.3390/molecules22020246.

Bentley, M.V.L., Marchetti, J.M., Ricardo, N., Ali-Abi, Z., Collett, J.H., 1999. Influence of lecithin on some physical chemical properties of poloxamer gels: rheological, microscopic and in vitro permeation studies. Int. J. Pharm. 193 (1), 49–55. https://doi.org/10.1016/s0378-5173(99)00313-0.

Biranje, S.S., Madiwale, P.V., Patankar, K.C., Chhabra, R., Dandekar-Jain, P., Adivarekar, R.V., 2019. Hemostasis and anti-necrotic activity of wound-healing dressing containing chitosan nanoparticles. Int. J. Biol. Macromol. 121, 936–946. https://doi.org/10.1016/j.ijbiomac.2018.10.125.

Calixto, G., Yoshii, A. C., Rocha E Silva, H., Stringhetti Ferreira Cury, B., Chorilli, M., 2015. Polyacrylic Acid Polymers Hydrogels Intended to Topical Drug Delivery: Preparation and Characterization. Pharm. Dev. Technol. 20, 490-496. https://doi.org/10.3109/10837450.2014.882941.

Cevher, E., Sensoy, D., Taha, M., Araman, A., 2008. Effect of thiolated polymers to textural and mucoadhesive properties of vaginal gel formulations prepared with polycarbophil and chitosan. Pharm. Sci. Tech. 9, 953–965. https://doi.org/10.1208/s12249-008-9132-y.

Czechowska-Biskup, R., Rokita, B., Ulański, P., Rosiak, J.M., 2015. Preparation of Gold Nanoparticles Stabilized by Chitosan Using Irradiation and Sonication Methods. Prog. Chem. Appl. Chitin and Its Derivat. 20, 18–33 https://doi.org/10.15259/PCACD.20.02.

Dalla, P., Faglia, E., 2006. Treatment of Diabetic Foot Ulcer: An overview Strategies for Clinical Approach. Curr. Diabetes Rev. 2, 431–447. https://doi.org/10.2174/157339981060204043 1.

Darweesh, R.S., Ayoub, M.N., Nazzal, S., 2019. Gold nanoparticles and angiogenesis: molecular mechanisms and biomedical applications. Inter. J. Nanomed. 14, 7643–7663. https://doi.org/10.2147/IJN.S223941.

De Matteis, V., 2017. Exposure to Inorganic Nanoparticles: Routes of Entry, Immune Response, Biodistribution and In Vitro/In Vivo Toxicity Evaluation. Toxics 5, 29. https://doi.org/10.3390/toxics5040029.

Encabo-Berzosa, M. del M., Sancho-Albero, M., Crespo, A., Andreu, V., Sebastian, V., Irusta S., Santamaria, J., 2017. The effect of PEGylated hollow gold nanoparticles on stem cell migration: potential application in tissue regeneration. Nanoscale. 9, 9848–9858. https://doi.org/10.1039/C7NR01853C.

Filon, F.L., Crosera, M., Adami, G., Bovenzi, M., Rossi, F., Maina, G., 2011. Human skin penetration of gold nanoparticles through intact and damaged skin. Nanotoxicol. 5, 493–501. https://doi.org/10.3109/17435390.2010.551428.

Geng, H., Song, H., Qi, J., Cui, D., 2011. Sustained release of VEGF from PLGA nanoparticles embedded thermo-sensitive hydrogel in full-thickness porcine bladder acellular matrix. Nanoscale Res Lett. 6, 312. https://doi.org/10.1186/1556-276X-6-312.

Grada, A., Otero-Viñas, M., Prieto-Castrillo, F., Obagi, Z., Falanga, V.J., 2017. Research techniques made simple: Analysis of collective cell migration using the wound healing assay. J. Invest. Dermatol. 137, 11–16. https://doi.org/10.1016/j.jid.2016.11.020.

Hurler, J., Engesland, André, Poorahmary, K., Bahador, Škalko-Basnet, N., 2012. Improved texture analysis for hydrogel characterization: Gel cohesiveness, adhesiveness, and hardness. J. App.l Polym. Sci. 125, 180-8. https://doi.org/10.1002/app.35414.

Hutanu, D., Frishberg, M.D., Guo, L., Darie, C.C., 2014. Recent applications of polyethylene glycols (PEGs) and PEG derivatives. Mod. Chem. Appl. 2, 1–6. https://doi.org/10.4172/2329-6798.1000132.

Ismail, S.k., Khan, M.A., Haque, A., Ghosh, S., Roy, D., Homechuadhuri, S., Alam, A., 2020, Synthesis of Gold and Silver Nanoparticles Using Malva Verticillata Leaves Extract: Study of Gold Nanoparticles Catalysed Reduction of Nitro-Schiff Bases and Antibacterial Activities of Silver Nanoparticles. Curr. Res. Green Sustain. Chem., in press. https://doi.org/10.1016/j.crgsc.2020.05.003.

Jones, S., Woolfson, A., Brown, F., 1997. Textural, viscoelastic and mucoadhesive properties of pharmaceutical gels composed of cellulose polymers. Int. J. Pharm. 151, 223–233. https://doi.org/10.1016/S0378-5173(97)04904-1.

Jones, S., Woolfson, A., Djokic, J., Coulter, W.A., 1996. Development and mechanical characterization of bioadhesive semi-solid, polymeric systems containing tetracycline for the treatment of periodontal diseases. Pharm Res. 13, 1734–1738. https://doi.org/10.1023/A:1016413428473.

Katas, H., Lim, C.S., Nor Azlan, A.Y.H., Buang, F., Mh Busra, M.F., 2019. Antibacterial activity of biosynthesized gold nanoparticles using biomolecules from *Lignosus rhinocerotis* and chitosan. Saudi Pharm. J. 27, 283–292. https://doi.org/10.1016/j.jsps.2018.11.010.

Katas, H., Mohd Amin, M.C.I., Moideen, N., Ng, L.Y., Megat Baharudin, P.A.A., 2017a. Cell Growth Inhibition Effect of DsiRNA Vectorised by Pectin-Coated Chitosan-Graphene Oxide Nanocomposites as Potential Therapy for Colon Cancer. J. Nanomater. 2017, 1–12. https://doi.org/10.1155/2017/4298218.

Katas, H., Wen, C.Y., Siddique, M.I., Hussain, Z., Mohd Fadhil, F.H., 2017b. Thermoresponsive curcumin/DsiRNA nanoparticle gels for the treatment of diabetic wounds: Synthesis and drug release. Ther. Deliv. 8, 137–150. https://doi.org/10.4155/tde-2016-0075.

Katas, H., Siang, T.T., Raja, M.A.G., 2017c. Topical temperature-sensitive gel containing DsiRNA-chitosan nanoparticles for potential treatment of skin cancer. Trends Med. Res. 12, 1–13. https://doi.org/10.3923/tmr.2017.1.13.

Kavita, K.V., 2014. Choice of wound care in diabetic foot ulcer: A practical approach. World J. Diab. 5, 546–556. https://doi.org/10.4239/wjd.v5.i4.546.

Kramaric, A., Resman, A., Kofler, B., Zmitek, J., 1992. Thermoreversible gel as a liquid pharmaceutical carrier for a galenic formulation. European Patent. EP 0 551 626 A1.

Lee, S.S., Tan, N.H., Fung, S.Y., Sim, S.M., Tan, C.S., Ng, S.T., 2014. Anti-inflammatory effect of the sclerotium of *Lignosus rhinocerotis* (Cooke) Ryvarden, the Tiger Milk mushroom. BMC Complement Altern. Med. 14, 359. https://doi.org/10.1186/1472-6882-14-359.

Loh, E.Y.X., Fauzi, M.B., Ng, M.H., Ng, P.Y., Ng, S.F., Ariffin, H., Mohd Amin, M.C.I., 2018. Cellular and Molecular Interaction of Human Dermal Fibroblasts with Bacterial Nanocellulose Composite Hydrogel for Tissue Regeneration. ACS Appl. Mater. Interfaces. 10, 39532–39543. https://doi.org/10.1021/acsami.8b16645.

Machado, H.A., Abercrombie, J.J., You, T., DeLuca, P.P., Leung, K.P., 2013. Release of a Wound-Healing Agent from PLGA Microspheres in a Thermosensitive Gel. BioMed. Res. Int. 2013, 1–11. https://doi.org/10.1155/2013/387863.

Mahmoud, N.N., Al-Kharabsheh, L.M., Khalil, E.A., Abu-Dahab, R., 2019. Interaction of Gold Nanorods with Human Dermal Fibroblasts: Cytotoxicity, Cellular Uptake, and Wound Healing. Nanomater. 9, 1131. https://doi.org/10.3390/nano9081131.

Marza, S., Magyari, K., Bogdan, S., Moldovan, M., Pestean, C., Nagy, A., Papuc, I., 2019. Skin wound regeneration with bioactive glass-gold nanoparticles ointment. Biomed. Mater. 14,. https://doi.org/10.1088/1748-605X/aafd7d 025011.

Nayak, M.P., 2014. Green Synthesis of Gold Nanoparticles Using *Solanus Lycopersicum* (TOMATO) Aqueous Extract. World J. Nano Sci. Technol. 3, 74–80.

Nimasajai, X.S.B., 2018. Review on General Effective & Theraapeutic Diabetic Wound Management. Curr. Res. Diabetic Obes. J. 8, 1–9 https://doi.org/10.19080/CRDOJ.2018.08.555743.

Petkova-Olsson, Y., Altunab, S., Ullsten, H., Jarnstrom, L., 2017. Temperature effect on the complex formation between Pluronic F127and starch. Carbohydr. Polym. 166, 264–270. https://doi.org/10.1016/j.carbpol.2017.02.012.

Pisal, S.S., Paradkar, A.R., Mahadik, K.R., Kadam, S.S., 2004. Pluronic gels for nasal delivery of vitamin B-12. Part I: Preformulation study. Int J Pharm. 270, 37–45. https://doi.org/10.1016/j.ijpharm.2003.10.005.

Rarokar, N.R., Saoji, S.D., Khedekar, P.B., 2018. Investigation of effectiveness of some extensively used polymers on thermoreversible properties of Pluronic® tri-block copolymers. J. Drug Deliv. Sci. Technol. 44, 220–230. https://doi.org/10.1016/j.jddst.2017.12.002.

Rissanen, T.T., Vajanto, I., Yia-Herttuala, S., 2001. Gene therapy for therapeutics angiogenesis in critically ischemic lower limb - On the way to clinic. Eur. J. Clin. Invest. 31, 651–666. https://doi.org/10.1046/j.1365-2362.2001.00864.x.

Sarwar, A., Katas, H., Samsudin, S.N., Zin, N.M., 2015. Regioselective sequential modification of chitosan via azide-alkyne click reaction: synthesis, characterization, and antimicrobial activity of chitosan derivatives and nanoparticles. PlosOne. 10,. https://doi.org/10.1371/journal.pone.0123084 e0123084.

Steckiewicz, K.P., Barcinska, E., Malankowska, A., Zauszkiewicz-Pawlak, A., Nowaczyk, G., Zaleska-Medynska, A., Inkielewicz-Stepniak, I., 2019. Impact of gold nanoparticles shape on their cytotoxicity against human osteoblast and osteosarcoma in in vitro model. Evaluation of the safety of use and anti-cancer potential. J. Mater. Sci Mater. Med. 30, 22. https://doi.org/10.1007/s10856-019-6221-2.

Syeda, M.M., Jing, X., Mirza, R.H., Yu, H., Sellers, R.H., Chi, Y., 2012. Prostaglandin Transporter Modulates Wound Healing in Diabetes by Regulating Prostaglandin-Induced Angiogenesis. Am. J. Pathol. 181, 334–346. https://doi.org/10.1016/j.ajpath.2012.03.012.

Tahar, I.B., Fickers, P., Dziedzic, A., Płoch, D., Skóra, B., Kus-Liśkiewicz, M., 2019. Green pyomelanin-mediated synthesis of gold nanoparticles: modelling and design, physico-chemical and biological characteristics. Microb. Cell Fact. 18, 210. https://doi.org/10.1186/s12934-019-1254-2.

Vieira, L.F. de A., Lins, M.P., Viana, I.M.M.N., dos Santos, J.E., Smaniotto, S., Reis, M.D. dos S., 2017. Metallic nanoparticles reduce the migration of human fibroblasts in vitro. Nanoscale Res. Lett., 12, 200. https://doi.org/10.1186/s11671-017-1982-3.

Volkova, N., Yukhta, M., Pavlovich, O., Goltsev, A., 2016. Application of Cryopreserved Fibroblast Culture with Au Nanoparticles to Treat Burns. Nanoscale Res. Lett. 11 (1). https://doi.org/10.1186/s11671-016-1242-y.

Yap, H.-Y.Y., Chooi, Y.-H., Firdaus-Raih, M., Fung, S.-Y., Ng, S.-T., Tan, C.-S., Tan, N.-H., 2014. The genome of the Tiger Milk mushroom, *Lignosus rhinocerotis*, provides insights into the genetic basis of its medicinal properties. BMC Genomics 15, 635. https://doi.org/10.1186/1471-2164-15-635.

Zhang, C., He, Y., Chen, Z., Shi, J., Qu, Y., Zhang, J., 2019. Effect of Polysaccharides from Bletilla striata on the Healing of Dermal Wounds in Mice. Evidence-based Complimentary and Alternative Medicine. 2019, Article ID 9212314. https://doi.org/10.1155/2019/9212314.